A year of internal Poincaré waves in southern Lake Michigan

Jun Choi,[1] Cary D. Troy,[1] Tsung-Chan Hsieh,[1] Nathan Hawley,[2] and Michael J. McCormick[3]

Received 14 February 2012; revised 21 May 2012; accepted 30 May 2012; published 18 July 2012.

[1] A unique set of full year, deep water observations from the middle of Lake Michigan's southern basin are analyzed to quantify the seasonal variability of the dominant near-inertial internal Poincaré wave. At this mid-lake location, the Poincaré wave is seen to describe more than 80% of the observed surface current variability for much of the year, with characteristic near-inertial frequency and clockwise-rotating velocities. The dominance of the near-inertial seiche on the flow decreases with depth. The wave persists during the "stratified period," roughly May through late December, and is supported by as few as 1–2 degrees of thermal stratification over 150 m; only after complete water column mixing does the wave go dormant for January through April. The strongest Poincaré wave activity is seen to correspond to the period of strongest summer thermal stratification (August), in spite of the relatively weak winds at this time. A simple inertial slab model optimized with linear friction is shown to capture the seasonal variability of the near-inertial energy at this location reasonably well. The vertical structure of the wave shows good agreement with that calculated with a standard normal modes formulation, which is in turn used to characterize the potential shear and mixing caused by the wave. Late-spring and summer events of elevated Poincaré wave activity are shown to generate sufficiently strong shear with persistent periods of sub-1 Richardson numbers within the thermocline, suggesting that the near-inertial seiche is likely generating thermocline instabilities in the lake's interior.

Citation: Choi, J., C. D. Troy, T.-C. Hsieh, N. Hawley, and M. J. McCormick (2012), A year of internal Poincaré waves in southern Lake Michigan, *J. Geophys. Res.*, *117*, C07014, doi:10.1029/2012JC007984.

1. Introduction

[2] In large stratified lakes, the effect of the earth's rotation has a pronounced influence on the character of the dominant wind-generated internal seiches [*Csanady*, 1972; *Antenucci and Imberger*, 2001, hereafter AI 2001; *Mortimer*, 2004, 2006]. Rotational seiches have been shown to enhance lateral dispersion [*Stocker and Imberger*, 2003], contribute significantly to basin scale mixing [*Gómez-Giraldo et al.*, 2006], and greatly enhance nearshore thermal variability [*Troy et al.*, 2012]. In the Great Lakes, the dominant rotational seiche is seen to dominate offshore currents [*Rao and Schwab*, 2007], and therefore likely plays a key in offshore dispersion of biota and pollutants.

[3] Two types of basin scale internal waves are typically seen in large stratified lakes: (1) shore-trapped internal Kelvin waves, which have largest influence nearshore and decay offshore with the scale of the internal Rossby radius (e.g., *Beletsky et al.* [1997] and *Mortimer* [2004] for Lake Michigan); and (2) internal Poincaré waves, which induce horizontal motion across the entire lake. These waves have their largest induced velocities in the lake's interior and vanishing influence nearshore (AI 2001). Our focus here is on internal Poincaré waves, which we show dominate the motion in Lake Michigan's interior for much of the year.

[4] The relative importance of rotation on internal seiches is captured by the Burger number, defined as $S_i \equiv c_i/fL$, where c_i is the long internal wave speed, f is the Coriolis parameter (e.g., $10^{-4}\ s^{-1}$ as for Lake Michigan, the focus of this study) and L is a horizontal length scale of the basin, e.g., the lake radius for an idealized circular lake (AI 2001). As a stratified lake becomes very large ($S_i \to 0$), the influence of Kelvin waves is restricted to a relatively thin nearshore zone, whereas the Poincaré wave dominates the majority of seiche-induced motion in the lake's interior. Also, for very large lakes, the theoretical Kelvin wave period becomes very large (e.g., 1 month for Lake Michigan) relative to meteorological variability, and no periodic signature of internal Kelvin waves is typically seen [*Troy et al.*, 2012].

[5] For truly large lakes where $S_i \to 0$, the periods of the various permissible Poincaré modes converge to the inertial period, and the energy in these near-inertial modes is primarily in the form of horizontal kinetic energy with only

[1]School of Civil Engineering, Purdue University, West Lafayette, Indiana, USA.
[2]Great Lakes Environmental Research Laboratory, NOAA, Ann Arbor, Michigan, USA.
[3]Cooperative Institute for Limnology and Ecosystems Research, University of Michigan, Ann Arbor, Michigan, USA.

Corresponding author: C. D. Troy, School of Civil Engineering, Purdue University, 550 Stadium Mall Dr., West Lafayette, IN 47907-20519, USA. (troy@purdue.edu)

0148-0227/12/2012JC007984

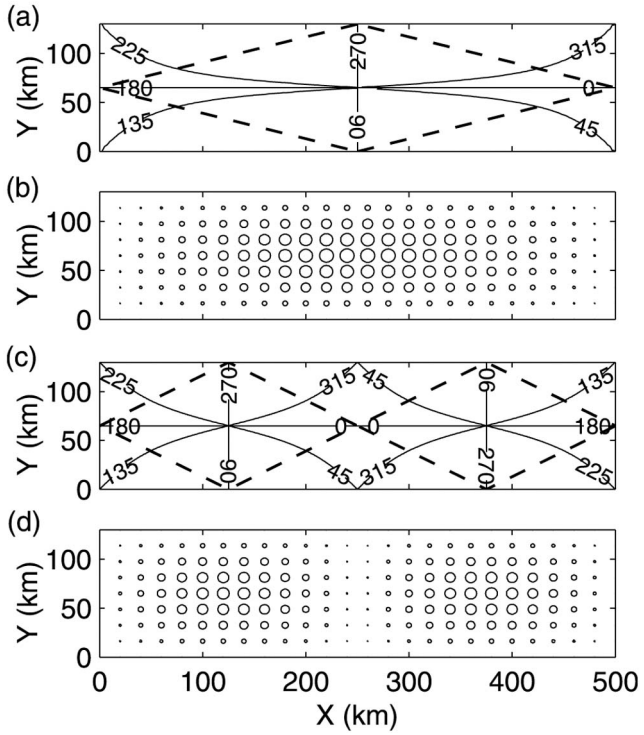

Figure 1. The gravest modes of internal Poincaré wave solutions [after *Csanady*, 1968; *Antenucci and Imberger*, 2001; *Mortimer*, 2004] for flat-bottomed, stratified rectangular basin (500 km × 130 km, roughly the size of Lake Michigan). Shown are (a and b) a single-celled mode and (c and d) a double-celled mode. The propagations of phase (solid lines) and maximum amplitude (dotted lines) of isotherm displacement for the rectangular basin are shown in Figures 1a and 1c, with the trajectories of particles during a period displayed in Figures 1b and 1d. The periods of the modes are 17.55 hrs for the single-celled mode and 17.52 hrs for the double-celled mode.

modest vertical displacements of the thermocline [*Mortimer*, 2004; AI 2001]. This is the case for Lake Michigan, the focus of the work described herein, for which the Burger number remains $O(10^{-2})$ or less for most of the year.

[6] While many vertical/horizontal/azimuthal internal Poincaré modes are possible (AI 2001), in general the lowest modes prevail, because it is the lowest modes that are most excited by a spatially uniform wind stress [*Csanady*, 1972]. The structure of the lowest two longitudinal modes in an ideal rectangular stratified basin, highlighted in Figure 1, have largest velocities in the lake center, with velocities everywhere in phase across the basin, rotating clockwise (in the northern hemisphere) at near-inertial period. Higher lateral modes in real basins can take the form of additional, similarly characterized, rotating cells in the basin, i.e., a single cell for the lowest mode and two cells for the second mode, etc. This was shown theoretically by *Schwab* [1977] for Lake Ontario and simulated by *Gómez-Giraldo et al.* [2006] for Lake Kinneret. Because the lowest Poincaré modes for very large lakes have similar, near-inertial periods, observation-based spectral determination of various unique modes is not always possible, especially in light of the seasonal variation of the thermal stratification that in turns causes seasonal variation in the periods. Unpublished, ongoing numerical simulations suggest that Lake Michigan's fundamental Poincaré response is a combination of a whole-basin mode and a two-basin (North/South) mode, similar to those described by *Schwab* [1977] for Lake Erie, although *Mortimer* [2004, 2006] found higher transverse modes in Lake Michigan and these are also likely present at times.

[7] For reference, the work described herein describes measurements near the deep center of Lake Michigan's southern basin; following the Poincaré structure described above, this is the location where the lowest modes should induce the largest surface currents and the smallest thermocline displacements. The local inertial period at the mooring is 17.7 h.

[8] Because both wind and thermal stratification vary strongly with seasons, the internal Poincaré wave characteristics manifested in the Laurentian Great Lakes are expected to exhibit strong seasonal variability, with corresponding seasonal variability in the wave's impact on transport and mixing. However, the two required ingredients for internal Poincaré waves – wind and thermal stratification – have opposite seasonal patterns for Lake Michigan, with the strongest winds during the unstratified winter/spring period and weak winds during the strongly stratified summer period. Unfortunately, many measurements are restricted to the summer period because of logistical constraints, and therefore the seasonal effects of wind and stratification on the dominant internal seiche are not well-understood in the Great Lakes.

[9] In this paper we utilize a unique full-year mooring data set from Lake Michigan's interior in order to examine the seasonal variability of near-inertial Poincaré wave activity in the lake. The paper is organized as follows: Section 2 describes the observations used in the analysis; Section 3 describes the seasonal variability inferred from the observations and attempts to recreate this variability with a simple slab model; we also present the vertical structure of the wave-induced currents, and examine the potential for wave-induced vertical mixing. Section 4 restates our fundamental conclusions and discusses the results; and Section 5 concludes with some hypotheses and future work related to the role of near-inertial Poincaré waves in basin-scale mixing and energetics.

2. Measurements and Methods

[10] The measurements described in this paper were taken as part of the Episodic Events in Great Lakes Experiment (EEGLE), a large multidisciplinary project examining the role of episodic events – generally winter storms – on the nearshore and offshore transport of biogeochemically important materials in the Great Lakes [*Green and Eadie*, 2004]. The experiment involved an array of physical observations during 1998–1999 in Lake Michigan including moored temperature chains, single point velocity meters, whole water column acoustic Doppler current profilers (ADCP), wave measurements, and standard meteorological observations. All of the data are archived at http://www.glerl.noaa.gov/eegle/data/data.html.

[11] In this paper we focus on the measurements of temperatures and velocities in the middle of Lake Michigan's

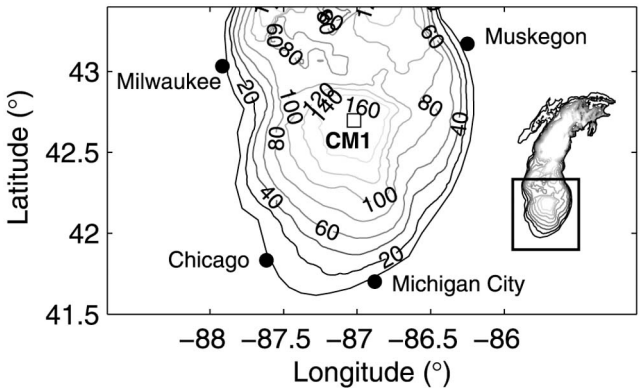

Figure 2. Lake Michigan and mooring CM1 location. Instruments at mooring CM1 included an array of single point vector-averaging current meters placed at 12, 22, 57, 117, and 154 m depths, with thermistors placed at 17, 27, 32, 37, 47, 77, 87, 97, 107, and 154 m depths.

southern basin at station CM1, which was located at 42 41.76′ N, 87 01.25′ W, and had a water depth of 154 m (Figure 2). The measurement period spanned just over one year, from 15 May 1998 to 2 June 1999. Instruments at mooring CM1 included an array of single point vector-averaging current meters (EG&G VACM) placed at 12, 22, 57, 117, and 154 m depths (hereafter denoted CM1–12, CM1–22, CM1–57, CM1–117, and CM1–154 respectively), which were sampled at 15 min intervals. CM1–57 returned only about one month of data and is not used in our analysis. Temperature measurements were also made continuously over the whole water column during the same period, with thermistors placed at 17, 27, 32, 37, 47, 77, 87, 97, 107, and 154 m depths. A nearby meteorological buoy measured wind and air properties, as well as water surface temperature, except for a brief period during winter. Additional measurements were taken at various locations around the lake, but are not utilized here.

[12] As a brief introduction to the data analyzed in this paper, the raw currents, wind stress, and temperatures at the mid-lake mooring are displayed in Figure 3. Wind and stratification show the typical seasonal variability experienced in Lake Michigan, with mid-lake thermal stratification beginning in May and strengthening through September, with a mixed layer depth of 15–20 m. Bottom waters at this location remain near 4°C for most of the year, and full turnover is not seen until roughly 1 Jan 1999 (Julian day 1 of 1999, hereafter "DOY," e.g., DOY 1 1999). Wind is weakest in summer, with the strongest winds occurring from November through March. Eastward and northward currents at this location are seen to be of roughly equal magnitude, and strongest during the summer period, when winds are generally weak but thermal stratification is strong. The magnitude of the observed currents decreases with depth in the water column, especially during the strongly stratified period.

[13] Ice records from the winter of 1998–1999 indicate that ice cover over the majority of the lake was minimal for the entirety of the winter, with ice only forming in Green Bay and the far northern shore of the lake.

[14] In order to isolate the velocities associated with the near-inertial internal Poincaré seiche, we employ a phase-preserving Butterworth band-pass filter centered on a period of 17.5 h with a band width of 4 h for much of the analysis. Several filters and filter types were tested in order to ensure that the results were not filter-dependent. For the majority of the year we show that the current record at CM1 is so

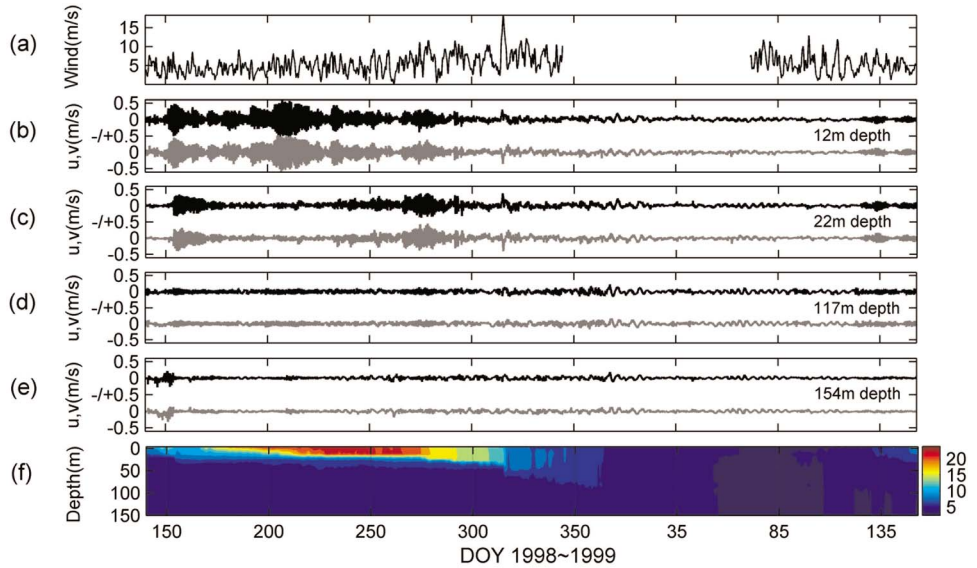

Figure 3. Wind speed, currents, and thermal stratification for mid-lake location in Lake Michigan's southern basin, years 1998–1999. Shown are (a) measured wind speed, and raw measured currents (gray: northward; black: eastward) from (b) 12 m depth, (c) 22 m depth, (d) 117 m depth, and (e) 154 m depth (near-bottom). (f) Full water column temperatures. Energy is seen to clearly decay with depth, with currents roughly equal in the north/east directions during the stratified period.

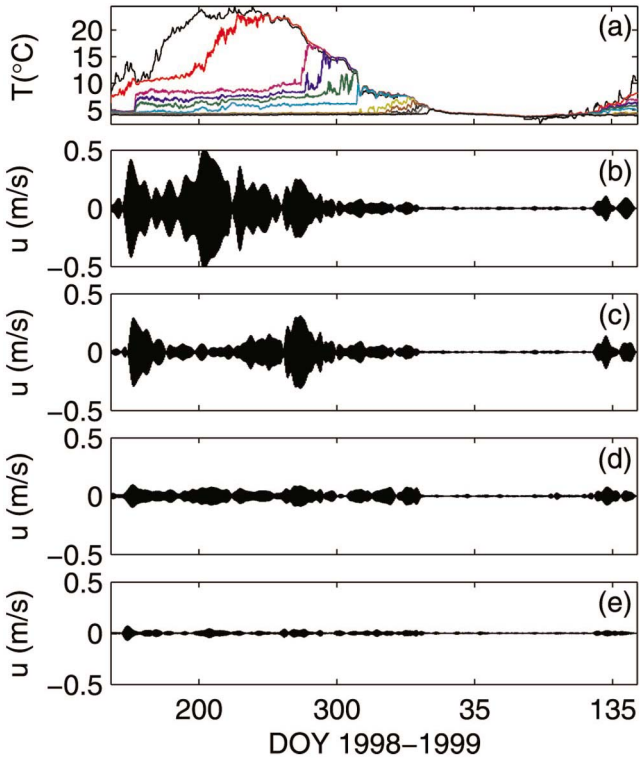

Figure 4. Water temperatures and near-inertial currents. Water temperatures are shown (a) at surface, 17, 27, 32, 37, 47, 77, 87, 97, 107, and 154 m depths. Band-passed (near-inertial) eastward currents from (b) 12 m depth, (c) 22 m depth, (d) 117 m depth, and (e) 154 m depth. Near-inertial currents are largest with the strongest thermal stratification, disappearing only upon complete homogenization of the water column (approximately January 1). Northward currents (not shown) appear identical when viewed at this scale, because the near-inertial seiche induces clockwise-rotating velocities of roughly equal magnitude.

thoroughly dominated by the near-inertial Poincaré seiche that the effect of band-passing the data is primarily to remove spurious high-frequency noise, with the exception of the brief unstratified period (Jan-March), during which the Poincaré wave is largely absent. We additionally apply the Hilbert transform to the band-passed data in order to infer the time-varying amplitude, period, and phase of the wave-induced velocities and temperatures.

3. Observations and Analysis of Near-Inertial Seiche

3.1. Basic Characteristics

[15] The near-inertial (band-passed filtered) currents from CM1–12 are shown in Figure 4. The dominance of the near-inertial seiche at the mid-lake location can be seen for most of the year (in comparison with the raw data shown in Figure 3; this domination is quantified subsequently). The envelopes of the eastward and northward velocity time series are nearly identical for this period of domination, in keeping with the expected roughly circular, clockwise-rotating velocity orbits associated with the near-inertial seiche in a large stratified basin [*Mortimer*, 2004, 2006; AI 2001]. Rotary wavelet analysis (not shown) performed on the currents shows that all perceivable energy in near-inertial frequencies lies solely in the clockwise-rotating spectrum.

[16] Near-inertial currents are seen to begin in May, when the measurements began, and the induced surface currents peak in late July and early August. Although winds increase into the fall and winter period, the near-inertial energy steadily decreases, until it disappears almost entirely at DOY 1 1999, which corresponds to the complete homogenization (turnover) of the water column. At this point, the top-bottom temperature difference over 150 m of water is less than 1 degree. Near-inertial activity again resumes as soon as a small vertical temperature contrast develops, which occurred at roughly DOY 130 in 1999, as seen by the temperature records also shown in Figure 4.

[17] The relationship between the near-inertial surface current and those at various other depths is not constant through the year, which is also seen in Figure 4; we show later that this is because the vertical (modal) structure of the wave-induced currents is set by the stratification, which evolves seasonally. For example, the modal shape during the mid-summer (e.g., DOY 200) has very strong vertical shear over the top portion of the water column, leading to very large near-surface velocities relative to those at deeper depths.

[18] A representative subset of the raw (unfiltered) time series, taken from the most strongly stratified period, is displayed in Figure 5, to illustrate the perfectly periodic nature of the signal at the mid-lake location (this pure periodicity can be seen upon closer inspection to a large degree for the entire period of Poincaré domination). The velocities are also seen to be *extremely* large (for the entirely wind-driven Great Lakes), approaching 50 cm/s at this location, for a prolonged period. The associated particle pathline illustrates the clockwise-rotating nature of the velocities, and the near-circular particle orbits additionally highlight the equality between the induced eastward and northward currents, as well as the lack of other processes influencing motion at this location during this period. For example, neglecting lateral variations in the velocity field, during the period DOY 200–220, a particle released in the mixed layer near CM1 would have traveled almost 700 km - nearly twice the north-south length of Lake Michigan – to end up only 40 km from its original location.

[19] The period of the seiche was calculated as a function of the time of year, by fitting lines to subsets of the Hilbert transform-derived phase of the band-passed currents at 12 m depth (Figure 6); other depths showed similar periods and temporal variability. As shown by AI 2001 and *Mortimer* [2004, 2006], the periods of the fundamental Poincaré modes converge to the inertial period as the Burger number approaches zero (weakest stratification), and decrease as stratification strengthens. Figure 6 shows that for the period during which the lake is strongly stratified, the identified period of the dominant seiche(s) at CM1 is relatively constant at 17.4–17.5 h (the local inertial period at the measurement location is 17.7 h but varies north to south across Lake Michigan's full basin from 17.4 to 18.0 h, respectively [*Mortimer*, 2006]).

[20] The observed period agrees with that expected for the lowest Poincaré modes [*Mortimer*, 2006], in that it is nearly equal to the inertial period, which is to be expected for a lake

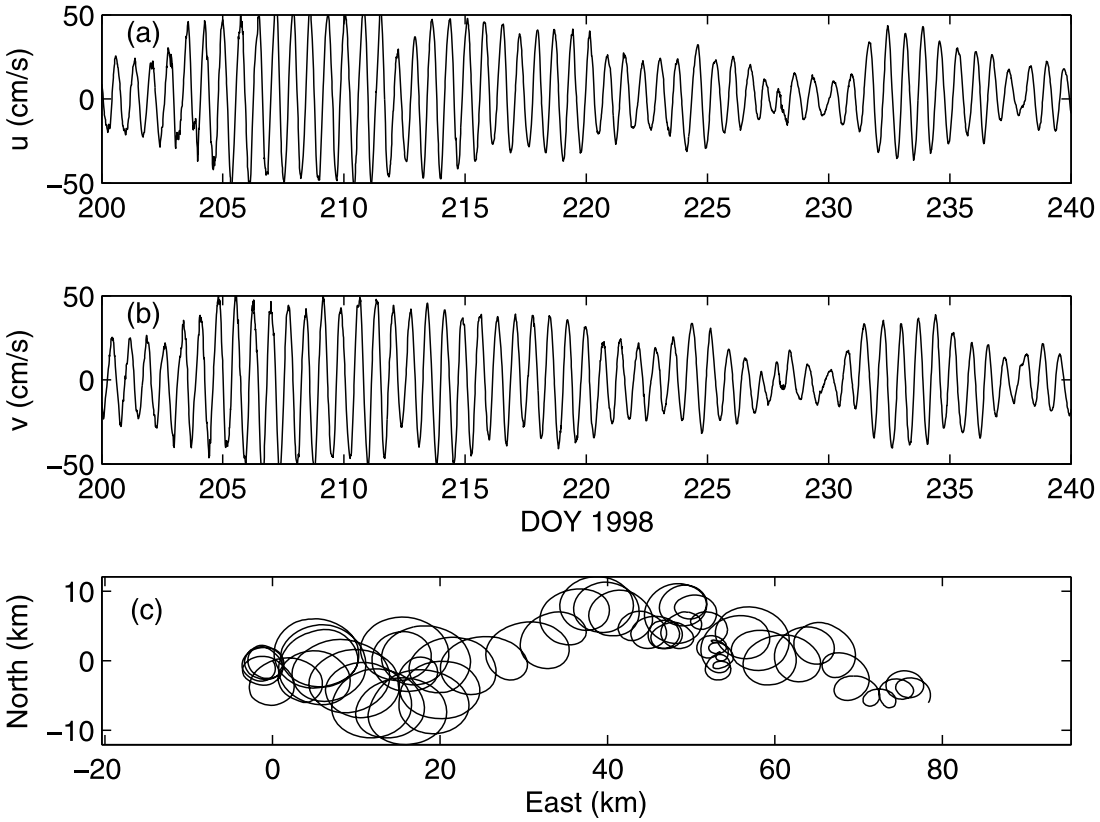

Figure 5. Raw (unfiltered) (a) eastward and (b) northward velocities and (c) associated particle pathline for strongly stratified period when Poincaré wave activity is most dominant at mid-lake location CM1. The sense of rotation for all of the orbits is clockwise and the dominant period is roughly 17.4 h.

as large as Lake Michigan. This spectrally perceived "dominant" period is likely a combination of the two lowest modes for the basin, as discussed later; the combination of the non-stationarity of the record (due to wind and stratification variability) and the nearly identical (nearly inertial) periods for the lowest Poincaré modes make spectral separation of the various modes extremely difficult, if not impossible [*Schwab*, 1977; *Mortimer*, 2004]. This is not an issue for smaller lakes for which spectra can be readily used to identify various fundamental Poincaré modes [e.g., *Antenucci et al.*, 2000]. Additionally, the method of using a fit to the Hilbert phase in order to infer the wave period is somewhat noisy, since the wave phase to some degree resets with strong wind events.

[21] The response to individual wind events is shown in Figure 7, which shows the near-inertial wave phase in response to wind-forcing during a subset of the data during the strongly stratified period. The phase is seen to shift slightly in response to strong wind events, as seen by shifts in the spacing between successive waves (e.g., DOY 228, 231), suggesting that to some degree the wave is slightly reset from strong winds. This is discussed further in Section 4. Wind-wave phase response is similar for the weakly stratified period (not shown), with the difference being that the Poincaré wave is so weak during that period that the phase is occasionally entirely reset by wind bursts, which are very strong and prolonged during the weakly stratified period.

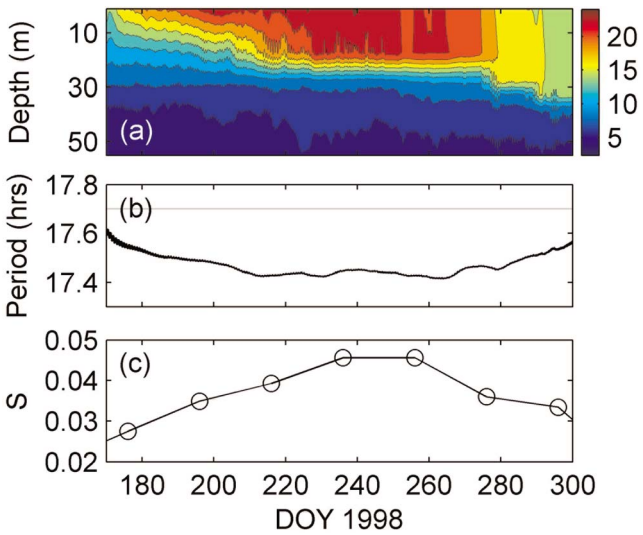

Figure 6. Dominant near-inertial period from the 12 m depth current measurements, as estimated with Hilbert transform. Shown are (a) water column temperatures; (b) dominant period, with local inertial period shown as gray line; and (c) estimated Burger number.

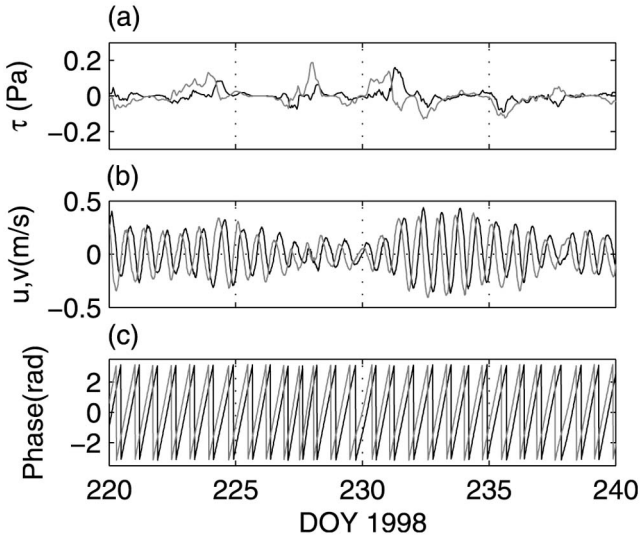

Figure 7. Wind stress, currents, and wave phase during the strongly stratified period. Shown are (a) eastward (black) and northward (gray) wind stress, (b) eastward (black) and northward (gray) raw currents, and (c) near-inertial wave phase obtained via Hilbert transform. Large wind bursts are seen to reset the Poincaré wave phase, e.g., DOY 228, and this may serve to keep multiple near-inertial modes aligned for most of the stratified period.

3.2. Seasonal Variability

3.2.1. Relative Dominance of Near-Inertial Seiche

[22] Velocity spectra are presented in Figure 8, for both the stratified and unstratified periods. The spectra again show the clear dominance of the near-inertial seiche during the stratified period, and the disappearance of this energy during the unstratified period.

[23] The spectra also show periodicity in a broad band centered at an approximately 90 h period, which matches the lowest "vortex mode" described by *Saylor et al.* [1980]. The relative strength of the 90 hr vortex mode is seen to be stronger for the deeper (117 m) depth, which is because the vortex mode is a barotropic feature, with near-uniform influence over depth, whereas the Poincaré wave is a baroclinic feature with minimal influence at great depths.

[24] Some additional energy is also seen at a period close to the near-inertial first harmonic (8.65 hrs); this harmonic is seen more in the near-surface currents (12 m depth), but it is not known whether this harmonic is an indication of wave nonlinearity. The waves are certainly not nonlinear with respect to wave steepness, with several meters of thermocline deflection across the O(10^2) km basin. The nonlinear advection term (e.g., $u\ \partial u/\partial x$) associated with these waves, however, which would generate energy at a near-inertial harmonic, should be of maximum order O($U/L\omega \sim 0.1$), where U is the velocity scale (0.5 m/s at maximum), L is the horizontal length scale (50 km), and ω is the wave period ($\omega \sim f$, $10^{-4}\ s^{-1}$). Therefore it is plausible that the waves may be weakly nonlinear during periods of strongly elevated energy.

[25] Although not shown, very concentrated energy is seen in the eastward velocity spectra at a period of 2.18 hrs, which corresponds with the east-west transverse barotropic seiche period of 2.19 h identified by *Mortimer and Fee* [1976] and 2.17 hrs calculated by *As-Salek and Schwab* [2004]. This energy is not seen in the northward velocity spectra (not shown), which seems to definitively identify this feature as the east-west barotropic seiche. It is interesting to note the difference in the character between the spectral peaks of the fundamental baroclinic (near-inertial) and barotropic (2 h) seiches. The barotropic seiche has a very narrow peak, since its frequency is set by the total water depth, which changes negligibly over the year; the baroclinic (Poincaré) seiche is much broader spectral peak, most likely because (1) the baroclinic period evolves seasonally with the stratification and (2) multiple near-inertial modes may influence the measurement location.

[26] The seasonal cycle of the relative dominance of the near-inertial seiche is highlighted in Figure 9, which shows the spectral energy in various spectral bands, including near-inertial (NI) and near-four-day (N4). The near-inertial seiche is seen to completely dominate the near-surface currents for the majority of the stratified period, containing more than 80% of the energy during the strongly stratified period of the year. The dominance is also seen readily by eye, simply looking at the raw currents (e.g., Figure 5).

[27] The influence of the near-inertial seiche is seen to decay with depth, with all depths following a similar seasonal variation, and nearly complete disappearance of the near-inertial seiche upon complete homogenization of the water column (DOY 1 1999). The variation in near-inertial energy with depth can be well-explained with the vertical structure of the lowest vertical mode, which has large near-surface velocities above the thermocline and very small velocities in the hypolimnium (this is discussed further in a subsequent section). At depth (154 m), the near-inertial seiche at its strongest is only responsible for at most 60% of the observed variability, suggesting that the lake bottom boundary layers in the deeper portions of the lake are not nearly as heavily influenced by the seiche (the seiche should, however, have increasing near-bottom influence as one considers shallower waters, in accordance with the cross-shelf evolution of the vertical structure of the wave).

3.2.2. Seasonal Stratification and Wind Stress Variations

[28] In terms of the thermal stratification, the internal Poincaré seiche is seen to be supported by top-bottom temperature differences of 1–2 degrees and greater, which coincides with the observed period of near-inertial currents (Figures 3 and 4). For the observations presented here, that spans the period except 1 Jan 1999 to 2 May 1999. The amount of energy absorbed by the near-inertial seiche appears to depend primarily on the strength of the stratification and only weakly on the wind stress magnitude, with the seasonal variability of the Poincaré wave-induced velocities following the seasonal stratification pattern, and not the seasonal wind stress pattern (Figure 10). This trend is noticeable in fall, when winds are relatively strong and stratification is still present, but yet the amount of energy in the basin-scale seiche is less than during the stronger-stratified, but weaker-winded summer period.

[29] Curiously, in winter, long-term observations at NOAA's buoy 45007 (located near CM-1) show the average over-lake wind speed is roughly double that of the summer

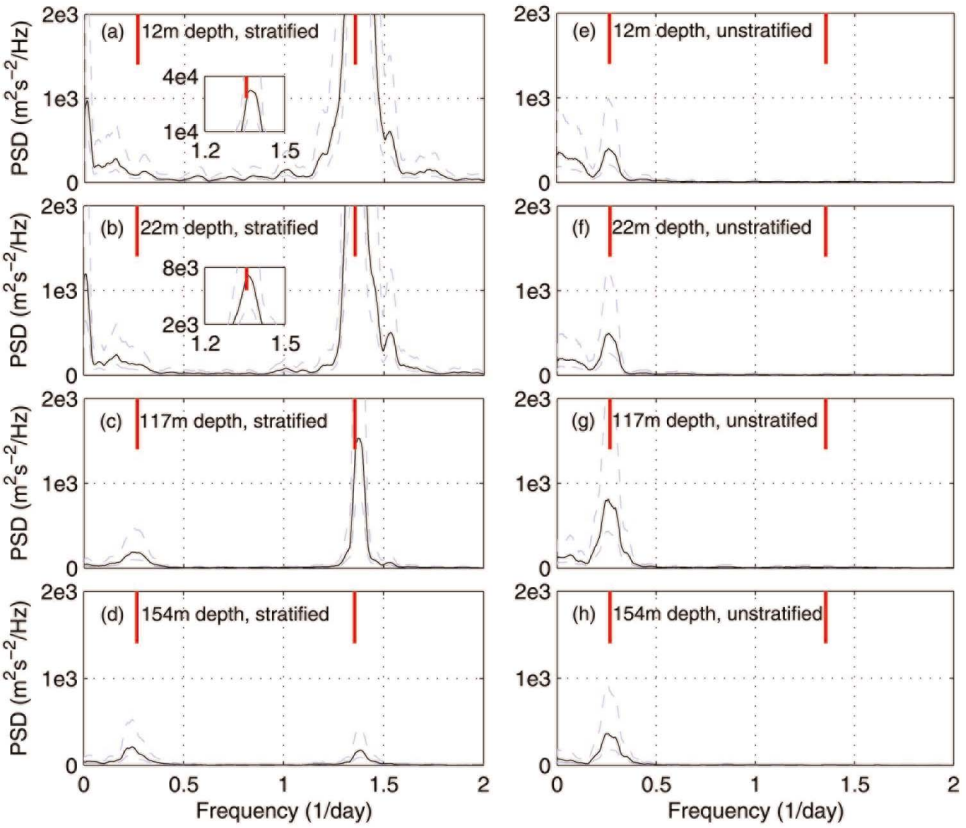

Figure 8. Eastward velocity spectra at 12 m, 22 m, 117 m, 154 m depths for stratified and unstratified seasons. The strongly stratified season refers to the period DOY 171–296 in 1998, and the unstratified season refers to the period DOY 15–108 on 1999. The two red lines are located at the periods of 90 h and 17.7 h (inertial period), corresponding to the southern basin vortex mode and near-inertial seiche, respectively. Gray lines indicate lines of 95% confidence. The maximum peaks are shown in the embedded windows in Figures 8a and 8b.

months (effectively quadrupling wind stress). Yet the mid-lake observations discussed here show that total kinetic energy is actually at a minimum during winter (e.g., Figures 3 and 9). Where does the increased energy go? At present we have only hypotheses, all of which represent energies not resolved by this data set. Spectrally, high-frequency processes (less than the sample period of 15 min), namely waves and turbulence, are not captured by this data set, although in general one can observe an elevation of the (resolved) high frequencies during winter. Surface waves at buoy 45007 are approximately 3–4 times as large in winter as in summer, and therefore represent a potential sink for the elevated wind energy imparted to the lake. Spatially, wind will preferentially accelerate shallow nearshore waters, in turn causing turbulence that will ultimately be dissipated; however, a cursory look at nearshore current records from 1998 to 1999 does not show greatly elevated currents during winter. Ongoing work seeks to place the present measurements in the context of the global lake energy budget and to determine the pathways of energy flux for the lake.

3.3. Slab Model

[30] An effort was made to explain the observed seasonal variability of the near-inertial seiche strength with the simplest model possible that would contain the primary ingredients to the seiche: wind and thermal stratification. Following *Pollard* and *Millard* [1970] and *D'Asaro* [1985], who modeled baroclinic near-inertial wave generation in the surface mixed layer, a simple slab model with linear friction was first attempted. The model equations for the depth-averaged mixed layer horizontal velocities (u, v) are:

$$\frac{du}{dt} - fv = \frac{\tau_x}{H\rho} - ru \tag{1}$$

$$\frac{dv}{dt} + fu = \frac{\tau_y}{H\rho} - rv \tag{2}$$

Here τ_x and τ_y are the eastward and northward components of wind stress, respectively; H is the surface mixed-layer thickness; ρ is the mixed-layer density; and r is linear friction coefficient. The fundamental response of this model is clockwise-rotating inertial oscillations that are damped with a time scale of $1/r$ The model is best suited for unbounded domains with negligible lateral variability, where pressure gradients are not important (in this way, one should argue that it is not suitable for the modeling of internal Poincaré waves). Nevertheless, it has proved successful at capturing basic characteristics of wind-driven flow in a variety of

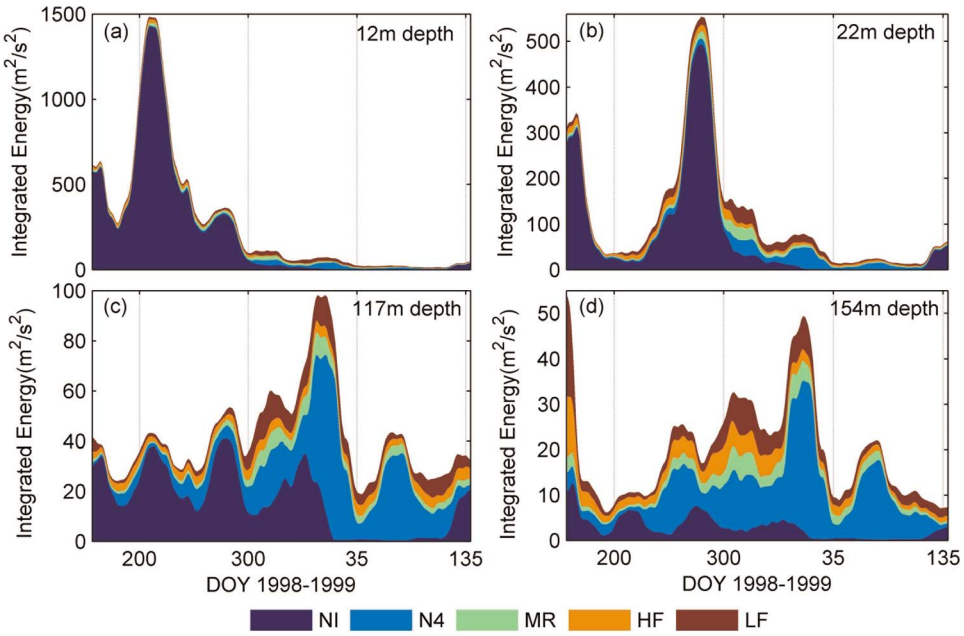

Figure 9. Seasonal variation of the relative energy of the near-inertial seiche (NI) and 4-day vortex modes (N4) [*Saylor et al.*, 1980], as quantified with monthly records. Also shown are the energies in the low-frequency (period > 125 h, LF); high-frequency (period < 15 h, HF); and middle range (20 hours < period < 65 hours, MR). Axes have been scaled differently to show the range of energies for a given depth. The dominance of the near-inertial seiche at this location is over 90% for almost the entire strongly stratified season, when winds are actually weakest; the 4-day vortex mode is seen to be strongest when winds are strongest.

oceanic settings [*MacKinnon and Gregg*, 2005], and the simplicity of the model makes it very attractive.

[31] To apply this model to the stratified portion of the measurement period where a mixed layer could be defined (DOY 220–320 of 1998), the wind stress was estimated using standard bulk coefficients applied to the observed winds; the mixed layer thickness was defined as the depth at which the maximum Brunt-Väisälä frequency occurred (defined in the usual manner as $N^2 \equiv -\frac{g}{\rho}\frac{d\rho}{dz}$), which was determined from the whole-water column thermal observations (Figure 3). Other definitions of mixed-layer thickness are obviously possible (e.g., isotherms and the zero-crossing of the normal modes profile), but the location of maximum stratification is defensible from the standpoint of the zero-stress assumption at the base of the mixed layer, since vertical turbulent momentum exchange (stress) would be most severely damped where thermal stratification was strongest. It is also straightforward to calculate with a standard vertical profile of temperature.

[32] The results of the slab model application are shown in Figure 11. Here the decay scale $1/r$ has been taken to be 10 days, in order to produce good agreement between the model and the observations. Figure 11 shows, surprisingly, that the slab model does actually reproduce much of the observed near-inertial variability, especially if one is interested in the seasonal trends of near-inertial energy. This is surprising for a number of reasons, given the numerous (invalid) assumptions in the slab model. That the model reproduces the *magnitudes* of the observed currents

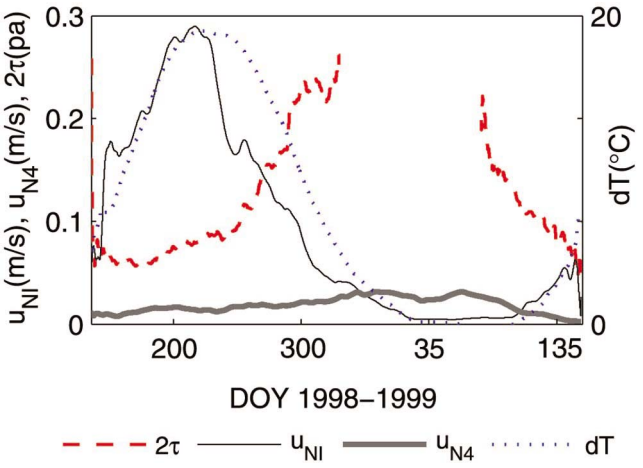

Figure 10. Seasonal variation of near-inertial currents (12 m depth), top-to-bottom temperature contrast, wind stress, and 90-h (vortex mode) currents. Near-inertial and vortex mode current magnitudes are obtained from the envelope of the Hilbert transform, with all time series smoothed to isolate seasonal variability. Wind stress has been doubled to scale to the chosen (left) axis. The variables τ, u_{NI}, u_{N4}, and dT indicate wind shear stress, near inertial current, near 4 days current, and the temperature difference between surface and bottom at CM1, respectively. Near-inertial energy is strongest when stratification is strongest and winds are at their weakest.

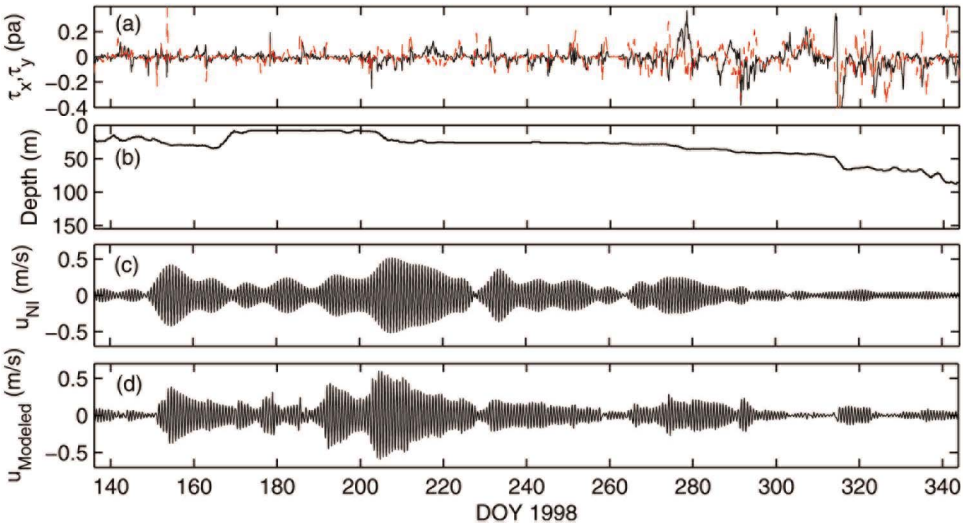

Figure 11. Slab model [e.g., *D'Asaro*, 1985] results and observations. Shown are (a) eastward (black) and northward (red) wind stress; (b) location of the base of the mixed layer, as defined by location of maximum buoyancy frequency N^2; (c) observed near inertial u current; and (d) modeled u current. A decay constant of 10 days of 1/r is used to give good agreement. Despite the extreme simplicity of the model, it performs well in capturing the seasonal variability in the near-inertial signal.

reasonably well seems to be a fortuitous fluke, given that with the radial variability in the Poincaré velocity field (Figure 1) it would then match poorly at locations closer to shore.

[33] Because the model's response is inertial, and the actual (observed) Poincaré wave is near-inertial, it would seem unlikely that such agreement would occur since the absorption of wind energy by the wave depends on the relative phase between wind and wave-induced currents. However, as found in the examination of the wind-phase relationship for the observations (Figure 7), the wind does appear to slightly "reset" the wave phase, and this periodic resetting may be significant enough to eliminate the need for the model to exactly capture (and retain) the wave phase. In essence, the Poincaré wave may be "inertial enough" that only minor drift occurs between waves of (modeled) inertial and (observed) near-inertial periods over several days before getting reset by another wind burst. The same idea may be true for multiple excited near-inertial modes in the lake: they may remain virtually perpetually phase-locked for most of the stratified season, drifting slightly, and then becoming realigned with the next wind burst.

[34] If one attempts to optimize the agreement between the observations and the model by tuning the decay constant throughout the year, the fitted decay timescale is seen to vary from 10 days during the strongly stratified period to 4 days when stratification is severely weakened at the end of the calendar year. The model does quite poorly during periods of very weak stratification, largely because the location of maximum N^2 – which was our choice for the mixed layer thickness - becomes ambiguous. It does appear that one of the primary reasons the slab model succeeds at capturing the seasonal variability of the Poincaré absorption of wind energy is that the model does capture the thickness of the mixed layer, which in turn determines the magnitude of the wave response (equations (1) and (2)). Additionally, most of the elevated winter wind energy is seen from spectra to be at low frequencies of several days and more, which one can show does not project efficiently onto the inertial slab model.

3.4. Vertical Structure and Potential Mixing

[35] While the 4 single point current measurements at the mooring do not provide extensive information on the vertical structure of the currents associated with the near-inertial Poincaré seiche, a simple normal modes model was applied to more completely infer this vertical structure, in order to quantify the seiche's influence on cross-thermocline shear

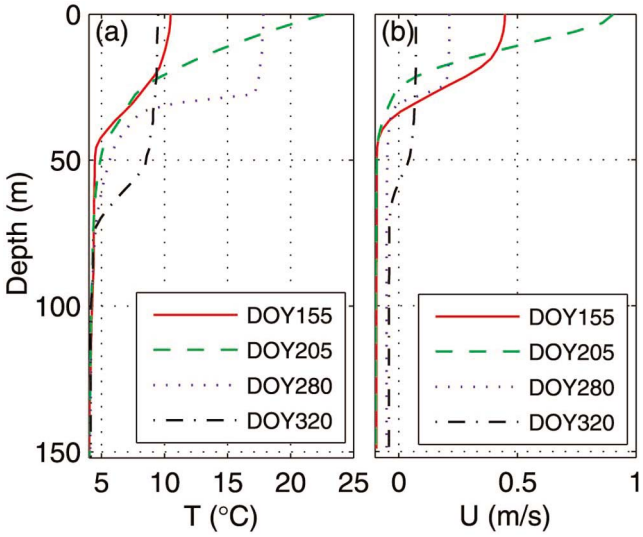

Figure 12. (a) Observed temperature profiles for various times of the stratified period, and (b) associated fitted normal modes solutions. Normal modes solutions in Figure 12b are scaled by observed near-inertial velocity magnitude at 12 m depth.

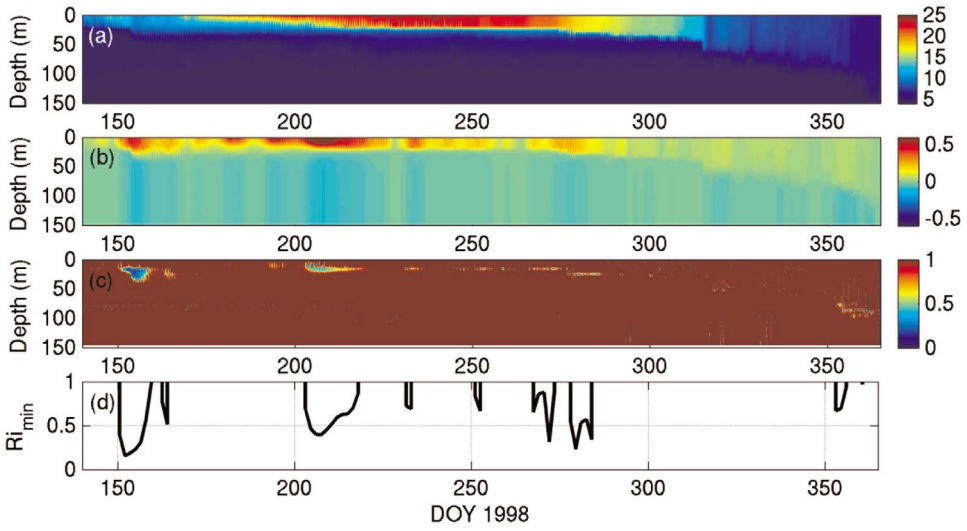

Figure 13. (a) Interpolated water column temperatures, (b) induced horizontal velocities calculated from fitted normal modes analysis, (c) associated Richardson number distribution, and (d) thermocline Richardson number.

and potential mixing. The linearized, inviscid, hydrostatic normal modes equation for a fluid with buoyancy frequency distribution N^2 is

$$\frac{d}{dz}\left(\frac{1}{N^2}\frac{d\psi_n}{dz}\right)+\frac{1}{c_n^2}\psi_n=0 \tag{3}$$

[e.g., *Kundu et al.*, 2012]. Here ψ_n(z) is the normal mode eigenfunction for the n^{th} baroclinic mode (from which the vertical and horizontal velocity functions are recovered), and c_n is the celerity of that mode. Underlying this equation is the assumption of separable wave-like solutions of the form $q = \Sigma q_n\,(x, y, t)\,\psi_n\,(z)$, where q is a dependent field variable (e.g., horizontal or vertical velocity u or w); once the eigenfunction $\psi(z)$ and eigenvalue c_n are found, the flow velocities themselves can be recovered via the normal mode equations.

[36] The normal modes solutions for horizontal velocity distributions were found numerically by solving (3) continuously in time for the observed thermal stratification, using the interpolated thermal stratification for N^2 (z). Only the first vertical mode was considered, because of its assumed dominance [e.g., *Csanady*, 1972] as well as the relatively coarsely spaced velocity measurements that could not resolve higher vertical modes. The solution of this equation yielded the horizontal velocity distributions $u(z)$ and $v(z)$, which were then scaled with the observed near-inertial current measurement magnitudes at 12 m depth (obtained from the envelope of the Hilbert transform) to obtain an estimate of the full water column Poincaré wave-induced velocity distribution at CM1.

[37] Figure 12 shows some sample observed thermal profiles and their associated scaled horizontal modal velocity profiles for various times during the year, including the very weakly stratified period. The normal modes solutions for the lowest mode yield largest velocities near the surface, with weak opposing velocities below the thermocline, as observed in the near-inertial currents (Figure 4); in general the velocity distributions mirror the thermal distributions. Maximum shear is concentrated in the thermocline, as expected. The root mean squared error between the fitted normal modes solutions and the raw currents at 22 m and 117 m depths were 5.2 cm/s and 1.5 cm/s, respectively, suggesting that the fitted normal modes give reasonable, but not perfect representations of the observed vertical structure.

[38] While linearized stratified shear instability can only be truly diagnosed by solving the Taylor-Goldstein equation for the observed shear and temperature profiles, the minimum Richardson number in the thermocline – where shear and stratification are largest - will generally govern the stability of the thermocline [e.g., *Troy and Koseff*, 2005]. The consequences of mid-lake, wave-generated turbulence are also large in the thermocline, which is traditionally a barrier to vertical exchange during the strongly stratified period.

[39] The gradient Richardson number is defined here as:

$$Ri(z,t)=\frac{N^2}{\frac{1}{2}\left[\left(\frac{\partial\hat{u}}{\partial z}\right)^2+\left(\frac{\partial\hat{v}}{\partial z}\right)^2\right]} \tag{4}$$

where $\hat{u}(z,t)$ and $\hat{v}(z,t)$ are the observation-scaled, slowly varying normal modes solutions for horizontal velocity as described above. The factor of 1/2 is an averaging factor that is present because the current fields $\hat{u}$ and $\hat{v}$ are the Hilbert transform magnitudes of the near-inertial fields, i.e., they change slowly with time with wave episodes but do not resolve individual near-inertial cycles. Implicit here is an assumption that while the velocity field rotates clockwise over a near-inertial period, the magnitude of the shear remains constant (for truly circular current fields, near-inertial periodicity in shear should only occur when other flow processes are added to the wave-induced flow).

[40] Figure 13 shows the calculated Richardson number distribution for the record, with color map scaling chosen to highlight episodes of sub-1 Richardson number. From the figure it is apparent that during times of elevated Poincaré wave activity, the Poincaré wave-induced shear on its own is likely sufficiently strong to generate shear instabilities in the

thermocline (e.g., DOY 150–160; 200–220; 265–275). During these times, the zone of appreciably low Richardson number is seen to be a broad region about the thermocline, while less-intense episodes are concentrated over a narrower vertical extent. The Richardson number in the unstratified portion of the water column is high, suggesting that the shear provided by the wave in the majority of the water column is too weak to generate turbulence.

[41] The two strongest (potential) mixing events (DOY 150–160 and DOY 200–220) occur, respectively, (a) in the late spring when stratification is still relatively weak and Poincaré wave activity is just commencing, and (b) in the mid-summer when stratification is strongest but Poincaré wave activity is also at its peak. These events are characterized by a broad vertical region, centered about the thermocline, with sub-1 Richardson numbers (Figure 13). The vertical thermistor spacing is not suitably fine to resolve any mixed layer deepening associated with these events.

[42] It must be emphasized again that these calculations are for the near-inertial wave only, as they are derived from normal modes profiles fitted to the near-inertial observations, and thus the calculations neglect other processes (e.g., barotropic seiches, topographic waves, wind-driven surface currents) that are likely present. However, the near-inertial seiche is likely the dominant mechanism causing mid-water shear at this deep location, as it is the dominant baroclinic process, and given the weak summer winds (which could generate shear at the base of the mixed layer). Additionally, provided a given process has a timescale comparable to, or greater than, the near-inertial period of the Poincaré wave, shear from other processes will be additive for some portion of the wave period, further lowering the Richardson numbers for that period, given the clockwise rotating nature of the velocity fields.

4. Discussion

[43] A unique whole-year set of current and thermal observations from deep water in Lake Michigan's southern basin has been analyzed to provide insight into the seasonal variability of the near-inertial internal Poincaré wavefield, which is seen to thoroughly dominate currents at this location. The data show a pronounced seasonal structure, with wave activity beginning in spring with the first local occurrence of thermal stratification (roughly May 1), strengthening through summer with maximum energy during early August, and weakening steadily throughfall. It is not until the complete homogenization of the water column – which occurred at approximately January 1 – that the wave goes dormant for the winter period.

[44] The seasonal cycle of the wave is seen to mirror the seasonal variability in the stratification, with the strongest Poincaré wave activity occurring when the top-to-bottom thermal stratification is maximum. Wind is of course the source of the near-inertial wave energy, but interestingly the near-inertial energy maximum occurs during mid-summer when winds are at a minimum.

[45] The dominance of the near-inertial seiche on surface currents at the measurement location (the center of Lake Michigan's southern basin) is complete, with more than 80% of the energy attributable to the seiche during its strongest period. The influence decreases with depth, in keeping with the normal modes for the water column. In keeping with theoretical solutions [*Csanady*, 1968; AI 2001] and observations in large lakes (e.g., *Mortimer* [2004, 2006] for Lake Michigan), the associated motions are clockwise-rotating motions at near-inertial periods, with near-surface currents as strong as 50 cm/s during the strongly stratified period. While multiple Poincaré modes may have possibly influenced the currents at the measurement location, spectra could not resolve separate near-inertial peaks. This is a general issue with the detection of Poincaré wave modes in very large lakes: all of the dominant periods are near-inertial, and spectral separation is virtually impossible given the additional complication of the non-stationarity of the wavefield.

[46] A simple slab model, forced by observed winds, was applied to the measurements in an attempt to re-create some of the observed seasonal variability. Surprisingly, when optimized, the model was able to re-create much of the observed seasonal variability during the stratified period. This is in spite of the model's neglect of a host of processes and effects potentially important in the transfer of wind energy to the Poincaré wavefield, including the spatial non-uniformity of the wind field, transfer of energy to the hypolimnium, boundary effects, and pressure gradients (the list does not stop here). Nevertheless, the model may provide some utility in a predictive sense for other systems. The decay timescale, when used as a temporally varying fitting parameter, varied from 10 days during the strongly stratified period to 5 days during weak, late-season stratification. It is believed that the model performs reasonably well because it does account for the varying mixed layer thickness, which is essentially the amount of water accelerated by the wind, as well as the temporal variability of the wind field, which has more energy at inertial timescales during the summer and less in the winter.

[47] Based on the model's success and an examination of wave episodes observed during the strongly stratified period, which generally lasted 5–10 days, it appears that strong wind events during the stratified period does reset the wave phase to some degree. If this is the case, multiple near-inertial Poincaré modes may essentially remain in phase for most of the summer period, drifting from one another only very slightly in between wind bursts due to their similar periods, with the next wind burst serving to restore phase alignment between different near-inertial modes (this would make spectral separation virtually impossible). This hypothesis could be further tested with idealized numerical simulations.

[48] While the vertical resolution of the measurements was not high (4 sensors), the observed vertical structure of the wave-induced currents matched reasonably well with the structure of the associated normal modes solutions for the observed thermal stratification. These solutions suggest a zone of elevated internal wave-induced shear over the top 30 m of the wave column. Corresponding analysis based on fitted (continuous) normal modes solutions was carried out in order to infer the wave-induced Richardson number, for the purpose of performing a preliminary assessment of the degree to which the near-inertial seiche may cause significant vertical mixing, at least locally, during the stratified period. The analysis suggests that the strongest Poincaré wave events do induce sufficiently strong thermocline shear ($Ri < 1$) for prolonged periods, further suggesting that

near-inertial Poincaré waves do likely generate thermocline instabilities. Further work is needed - ideally with vertically well-resolved current measurements (i.e., ADCP) and concurrent microstructure measurements - to fully characterize the role of the near-inertial seiche on vertical mixing in Lake Michigan, even at this single location.

5. Conclusion

[49] The year-round measurements and their analysis provide unique insight into the seasonal variability of near-inertial internal Poincaré wave activity, as perceived in deep water at the middle of Lake Michigan's southern basin. However, the extrapolation of these inferences to other locations – ultimately for the purpose of explaining basin-scale energetics and mixing – is heavily dependent on knowledge of the basin-scale structure of the fundamental Poincaré mode(s). Our (unpublished) numerical simulations suggest that the fundamental internal Poincaré response of Lake Michigan, at least in terms of induced surface currents, is a combination of several modes, with velocities in phase across most of the basin, decaying nearshore; this was also found by *Mortimer* [2004, 2006]. Ongoing work seeks to determine the spatial structure of the dominant near-inertial modes, especially in terms of the vertical shear associated with the fundamental modes, in order to scale-up direct measurements of shear and vertical mixing at discrete locations. To that end, additional direct measurements of microstructure are needed in the Great Lakes.

[50] The knowledge of how basin-scale vertical mixing occurs in the world's largest lakes (e.g., the Laurentian Great Lakes) is at present poor, owing to a lack of focused studies where turbulent microstructure is directly quantified. The growing consensus regarding basin-scale mixing in smaller lakes (and the ocean) is that boundary mixing plays a key role in the overall budget [*Wüest and Lorke*, 2003]; this is also found for lakes in which rotational effects are important [*Hodges et al.*, 2000]. Boundary-induced mixing will almost certainly be significant in the Laurentian Great Lakes given the strong nearshore currents that occur during the summer periods. However, there is little observational evidence in the Great Lakes to support the conceptual model of nonlinear shoaling internal waves causing elevated boundary mixing, as has been found for smaller lakes and the world's oceans. The relative role of Poincaré waves in the world's largest lakes, in terms of their contribution to basin-scale mixing, is therefore potentially much more significant than previously appreciated, given the seasonal dominance shown herein, the strong vertical shear associated with these waves, and the lateral extent over which they dominate currents. In the limit of a very large stratified lake, could basin-scale mixing be accomplished primarily in the lake's interior?

[51] **Acknowledgments.** We acknowledge the constructive comments of two anonymous reviewers who helped to improve the paper. We also thank the personnel of the Marine Instrumentation Laboratory at the Great Lakes Environmental Research Laboratory (GLERL) for preparing and downloading the current meters and crew of the RV Laurentian for assistance in deploying and retrieving them. This work was funded by the National Science Foundation, Division of Physical Oceanography grant OCE-1030842. This is GLERL contribution 1631.

References

Antenucci, J. P., and J. Imberger (2001), Energetics of long internal gravity waves in large lakes, *Limnol. Oceanogr.*, *46*, 1760–1773, doi:10.4319/lo.2001.46.7.1760.

Antenucci, J. P., J. Imberger, and A. Saggio (2000), Seasonal evolution of the basin-scale internal wave field in a large stratified lake, *Limnol. Oceanogr.*, *45*, 1621–1638, doi:10.4319/lo.2000.45.7.1621.

As-Salek, J., and D. Schwab (2004), High-frequency water level fluctuations in Lake Michigan, *J. Waterw. Port Coastal Ocean Eng.*, *130*, 45–53, doi:10.1061/(ASCE)0733-950X(2004)130:1(45).

Beletsky, D., W. P. O'Connor, D. J. Schwab, and D. E. Dietrich (1997), Numerical simulation of internal Kelvin waves and coastal upwelling fronts, *J. Phys. Oceanogr.*, *27*, 1197–1215, doi:10.1175/1520-0485(1997)027<1197:NSOIKW>2.0.CO;2.

Csanady, G. T. (1968), Motions in a model Great Lake due to a suddenly imposed wind, *J. Geophys. Res.*, *73*(20), 6435–6447, doi:10.1029/JB073i020p06435.

Csanady, G. T. (1972), Response of large stratified lakes to wind, *J. Phys. Oceanogr.*, *2*(1), 3–13, doi:10.1175/1520-0485(1972)002<0003:ROLSLT>2.0.CO;2.

D'Asaro, E. A. (1985), The energy flux from the wind to near-inertial motions in the surface mixed layer, *J. Phys. Oceanogr.*, *15*, 1043–1059, doi:10.1175/1520-0485(1985)015<1043:TEFFTW>2.0.CO;2.

Gómez-Giraldo, A., J. Imberger, and J. P. Antenucci (2006), Spatial structure of the dominant basin-scale internal waves in Lake Kinneret, *Limnol. Oceanogr.*, *51*, 229–246, doi:10.4319/lo.2006.51.1.0229.

Green, S. A., and B. J. Eadie (2004), Introduction to special section: Transport and transformation of biogeochemically important materials in coastal waters, *J. Geophys. Res.*, *109*, C10S01, doi:10.1029/2004JC002697.

Hodges, B. R., J. Imberger, A. Saggio, and K. Winters (2000), Modeling basin-scale internal waves in a stratified lake, *Limnol. Oceanogr.*, *45*(7), 1603–1620, doi:10.4319/lo.2000.45.7.1603.

Kundu, P. K., I. M. Cohen, and D. R. Dowling (2012), *Fluid Mechanics*, 5th ed., 891 pp., Elsevier, Amsterdam.

MacKinnon, J. A., and M. C. Gregg (2005), Near-inertial waves on the New England Shelf: The role of evolving stratification, turbulent dissipation, and bottom drag, *J. Phys. Oceanogr.*, *35*(12), 2408–2424, doi:10.1175/JPO2822.1.

Mortimer, C. H. (2004), *Lake Michigan in Motion-Responses of an Inland Sea to Weather, Earth-Spin, and Human Activities*, Univ. of Wis. Press, Madison.

Mortimer, C. H. (2006), Inertial oscillations and related internal beat pulsations and surges in Lakes Michigan and Ontario, *Limnol. Oceanogr.*, *51*(5), 1941–1955, doi:10.4319/lo.2006.51.5.1941.

Mortimer, C. H., and E. Fee (1976), Free-surface oscillations and tides of Lakes Michigan and Superior, *Philos. Trans. R. Soc. London, Ser. A*, *281*, 1–61.

Pollard, R. T., and R. C. Millard (1970), Comparison between observed and simulated wind-generated inertial oscillations, *Deep Sea Res.*, *17*, 813–821.

Rao, Y. R., and D. J. Schwab (2007), Transport and mixing between the coastal and offshore waters in the Great Lakes: A review, *J. Great Lakes Res.*, *33*, 202–218, doi:10.3394/0380-1330(2007)33[202:TAMBTC]2.0.CO;2.

Saylor, J., J. Huang, and R. Reid (1980), Vortex modes in southern Lake Michigan, *J. Phys. Oceanogr.*, *10*, 1814–1823, doi:10.1175/1520-0485(1980)010<1814:VMISLM>2.0.CO;2.

Schwab, D. J. (1977), Internal free oscillations in Lake Ontario, *Limnol. Oceanogr.*, *22*(4), 700–708, doi:10.4319/lo.1977.22.4.0700.

Stocker, R., and J. Imberger (2003), Energy partitioning and horizontal dispersion in a stratified rotating lake, *J. Phys. Oceanogr.*, *33*, 512–529, doi:10.1175/1520-0485(2003)033<0512:EPAHDI>2.0.CO;2.

Troy, C. D., and J. R. Koseff (2005), The instability and breaking of long internal waves, *J. Fluid Mech.*, *543*, 107–136, doi:10.1017/S0022112005006798.

Troy, C. D., S. Ahmed, N. Hawley, and A. Goodwell (2012), Cross-shelf thermal variability in southern Lake Michigan during the stratified periods, *J. Geophys. Res.*, *117*, C02028, doi:10.1029/2011JC007148.

Wüest, A., and A. Lorke (2003), Small-scale hydrodynamics in lakes, *Annu. Rev. Fluid Mech.*, *35*, 373–412.